Blending HVDC-Link Energy Storage and Offshore Wind Turbine Inertia for Fast Frequency Response

Adrià Junyent-Ferré, *Member, IEEE*, Yousef Pipelzadeh, *Member, IEEE*, and Tim C. Green, *Senior Member, IEEE*

***Abstract*—This paper explores the benefits of combining the dc-link energy storage of a voltage source converter-based high-voltage dc (VSC-HVDC) link and the kinetic energy storage from wind turbines to facilitate in fast primary frequency control and system inertia to an ac network. Alongside physical and analytical justifications, a method is proposed which blends the energy stored in the HVDC link with the power control capabilities of the wind turbines to provide frequency response that is fast while not requiring excessive volume of capacitance nor demanding performance requirements on the wind turbines.**

***Index Terms*—Automatic generation control, high-voltage dc (HVDC) transmission, power system dynamics, wind energy integration.**

I. Introduction

CONVENTIONAL ac grids rely on the inertial, primary, secondary, and tertiary responses to regulate the power balance of the grid while maintaining the system at its optimal operating point at different time scales [1]. When a sudden imbalance occurs, the inertial response limits the rate of change of frequency (ROCOF) during the first few seconds, thanks to the inherent dynamics of synchronous generators. The primary controllers stabilize the frequency afterwards by adjusting the loading of the prime movers in a proportional manner to the frequency error.

Unlike conventional power plants, most renewable generators are not interfaced to the grid through synchronous machines but through electronic power converters. Thus, they lack an inherent ability to contribute toward inertial response. Moreover, these systems usually operate at their maximum available power and do not participate in primary response. With further deployment of renewable generation systems anticipated in the near future, system operators have become more concerned about short-term stability problems and a growing interest in demanding inertial and primary response capabilities from renewable generation systems has become apparent [2], [3].

In recent times, major wind turbine manufacturers have added frequency response capabilities as a feature of their wind turbines and there exist a number of patents covering different aspects of the control methods they use [4], [5]. While primary response requires operating wind turbines below their maximum loading, inertial response can be obtained from the kinetic energy of the wind turbine. This was first proposed in [6] and has been further analyzed in the literature [7]–[9].

The development of voltage source converter-based high-voltage dc (VSC-HVDC) transmission enables building offshore wind farms (WFs) in far locations with good availability of wind resources and space. These WFs are decoupled from the grid by the HVDC link. Thus, wind turbines are unaware of the deviations of the frequency of the main grid and the grid-side VSC (GS-VSC) becomes the means through which frequency support services can be provided. Suitable control structures to implement these services are currently being discussed. Because of the long distance and the conversion stages involved in the HVDC transmission, there is a concern in respect to the reliability and the reaction time to effectively provide system inertia. In [10]–[12], the authors use the wind turbine frequency response capabilities. In order to make the system robust to the loss of communication between the GS-VSC and the WF-VSC, they proposed to translate the frequency of the main ac grid to an equivalent variation of the HVDC link voltage controlled by the GS-VSC which is sensed at the WF-VSC and communicated to the wind turbines. Moreover, in [12], the authors analyzed how such method could be used in a multiterminal system. A different approach was proposed in [13], where the authors suggested that the energy stored in the capacity of the HVDC link could be used alone to provide inertia support.

Using the energy stored in the HVDC link alone to provide inertial response has the advantage of providing a very fast response toward the main ac grid while reducing the stress of the wind turbines, but it has the significant disadvantage of requiring a very large capacitance to be comparable to conventional power plants. On the other hand, relying solely on the frequency response capabilities of the offshore wind turbines has the disadvantage of introducing delays and distortions to the response due to different information transmission stages existing between the frequency measurement at the GS-VSC and the wind turbine reaction.

In this paper, the authors propose the idea of blending the energy stored in the HVDC link with the power control capabilities of the wind turbines as an alternative to the aforementioned methods. This method can provide a fast frequency response toward the ac grid while not requiring excessive volume of capacitance nor high-performance requirements on the wind turbines.

Manuscript received December 20, 2013; revised May 14, 2014 and July 18, 2014; accepted September 12, 2014. Date of publication October 21, 2014; date of current version June 17, 2015. The work of A. Junyent-Ferré was supported by Engineering and Physical Sciences Research Council (EPSRC) under the project Enhanced Renewable Integration through Flexible Transmission Options (ERIFT) programme under Grant EP/K006312/1. The work of Y. Pipelzadeh was supported by the EPRSC Control for Energy and Sustainability programme under Grant EP/G066477/1. Paper no. TSTE-00566-2013.

The authors are with Electrical and Electronic Engineering Department, Imperial College London, London SW7 2AZ, U.K (e-mail: adria.junyent-ferre@imperial.ac.uk).

Digital Object Identifier 10.1109/TSTE.2014.2360147

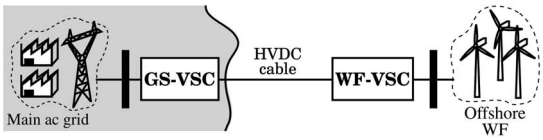

Fig. 1. HVDC-connected offshore WF scheme.

This paper is organized as follows: a model of the system is described in Section II. Frequency support requirements are discussed in Section III. A comparative analysis of the different methods for HVDC-connected WFs is presented in Section IV and the results of a detailed simulation test of the proposed method are discussed in Section V.

II. System Modeling

The analysis focuses on a point-to-point HVDC system where an offshore WF is connected to a WF-VSC which transfers the generated power to a GS-VSC connected to the main ac grid (see Fig. 1). In the first instance, a simplified model of the HVDC link is considered where the resistance of the cable is neglected along with its higher order dynamics. The adequacy of this assumption will be confirmed using high-order dynamic models for the simulation. Considering these assumptions, the dc-link voltage $V_{\rm dc}$ can be written as a function of the current injected by the converters as

$$\frac{d}{dt}V_{\rm dc} = \frac{1}{C}\left(i_{\rm wf} - i_{\rm gs}\right) \tag{1}$$

where C is the equivalent capacity of the link, wf refers to the WF side, and gs refers to the main ac GS of the link. The equivalent capacity of the system combines the energy stored in the dc capacitors of the converters along with the capacity of the cables. Transforming this equation by Laplace, we obtain

$$V_{\rm dc}(s) = \underbrace{-\frac{1}{Cs}}_{\triangleq G(s)} i_{\rm gs}(s) + \underbrace{\frac{1}{Cs}}_{\triangleq G_d(s)} i_{\rm wf}(s). \tag{2}$$

As a point-to-point connection, it is common to use a control scheme where the GS-VSC controls the dc-link voltage while the WF-VSC operates in the so-called V–f mode. When in V–f mode, the WF-VSC behaves as an ideal constant amplitude and constant frequency ac bus toward the WF collector by injecting an amount of power to the link dictated by the output power of the wind turbines.

A diagram of the closed-loop voltage regulation system is shown in Fig. 2. The closed-loop equation is

$$V_{\rm dc} = \underbrace{\frac{G(s)K(s)}{G(s)K(s)+1}}_{\triangleq G_T(s)} V_{\rm dc}^* + \underbrace{\frac{G_d(s)}{G(s)K(s)+1}}_{\triangleq G_S(s)G_d(s)} i_{\rm wf}. \tag{3}$$

The voltage regulator of the GS-VSC $K(s)$ is designed to provide the desired performance considering the operational limits of the converter along with the current that is expected to be injected by the WF-VSC.

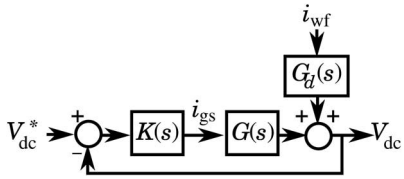

Fig. 2. Classic point-to-point HVDC link voltage control scheme.

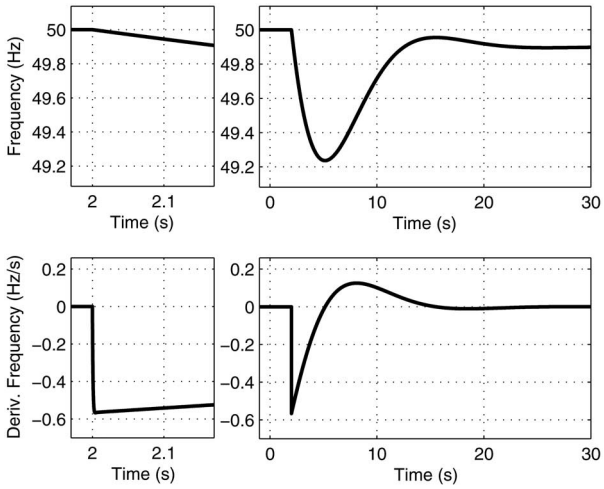

Fig. 3. Variation of the grid frequency and its derivative to a sudden increase of the load.

III. Frequency Support Power Reference Calculation

Providing short-term frequency support requires changing the power injected to the ac grid depending on the variation of its frequency. Two different terms have to be considered: one which is proportional to the ROCOF, which emulates the so-called inertial response of a synchronous machine, and the other which is proportional to error of the frequency, which corresponds to the primary control. An example of variation of these two variables when a step increase of the load occurs is shown in Fig. 3, as described in [14]. Notice that inertial response plays a major role in the recovery of the grid in the first few seconds after an event, whereas primary control has a slower response which can be seen during the first few tens of seconds afterwards.

The instantaneous value of the frequency of the grid can be obtained from the voltage measured at the Point of Common Coupling (PCC) of the GS-VSC. The resulting signal can be processed to obtain the power injection required to provide grid support. The inertial response term P_H^* can be calculated as [7]

$$P_H^* = -\frac{2HS^N}{\left(f^N\right)^2} f\frac{df}{dt} \approx -\frac{2HS^N}{f^N}\frac{df}{dt} \tag{4}$$

where H is the resulting emulated inertia time, S^N is the rated apparent power, and f^N is the nominal frequency of the grid. Equation (4) gives an estimation of the power headroom required from the converter to be able to provide a certain inertia time when running at rated power as a function of the maximum expected ROCOF $\dot{f}_R$

$$\frac{P_H^{\rm MAX}}{S^N} = -\frac{2H\cdot\dot{f}_R}{f^N}. \tag{5}$$

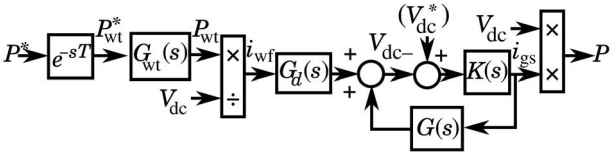

Fig. 4. Block diagram of Method I.

For example, for an inertia time of 2.5 s and a maximum ROCOF of 1 Hz $\cdot$ s^{-1} in a 50 Hz grid, the required headroom would be 10%.

This paper will focus on the analysis of inertial response, as inertial response has more critical time constraints. However, primary control features will be added to the detailed simulation model in Section V to ease the comparison at a longer time scale between a conventional ac system and an ac system with HVDC-connected WFs providing frequency support. The primary response term can be calculated as follows [7]:

$$P^*_{\rm gov} = K_{\rm droop}\left(f^N - f\right) \tag{6}$$

where $K_{\rm droop}$ is the steepness of the primary control characteristic.

IV. Obtaining Inertial Response From HVDC-Connected Offshore WFs

Three different methods will be discussed here: Method I, which relies on communicating the frequency to the wind turbines; Method II, which relies on using the energy of the HVDC link; and Method III, a new method which blends the energy stored in the HVDC link with the response of the wind turbines.

A. Method I: WF-Driven Response

The frequency of the grid is obtained by the GS-VSC and an order of variation of power is issued to the WF. The dynamics between the grid support power order and the actual power injected by the GS-VSC can be obtained by introducing the communication delay T and the wind turbine reference tracking dynamics $G_{\rm wf}(s)$ to the system model as shown in Fig. 4. The equivalent transfer function, considering small variations of $V_{\rm dc}$, becomes

$$P(s) = \underbrace{-K(s)G_S(s)G_d(s)}_{KS(s)G_d(s)} G_{\rm wt}(s)e^{-sT}P^*(s). \tag{7}$$

Thus, the system response to a power reference issued by the GS-VSC arises due to the cascaded effect of the communication stage, the wind turbine reference tracking dynamics, and the voltage regulation performance of the link $KS(s)G_d(s)$ [15].

The resulting response when a step increase in the power is required due to a sudden event happening in the ac grid is shown in Fig. 5. The simulation was carried out using a simplified model with the parameters summarized in Table I.

In a practical situation, no direct communication would exist between the GS-VSC and each individual wind turbine. The WF-VSC would have to transmit the signals from the GS-VSC to a WF controller which would dispatch the power order to each individual turbine depending on its state as proposed in [5]. Each of the steps would add additional lag to the response. Thus, the communications would be the predominant source of delay when using this method. This would potentially undermine the capability of the system to provide support during the first periods after a contingency, where the ROCOF depends on the inertia of the grid [14]. However, it has been shown in [10] that the system would still be capable of improving the minimum value reached by the frequency.

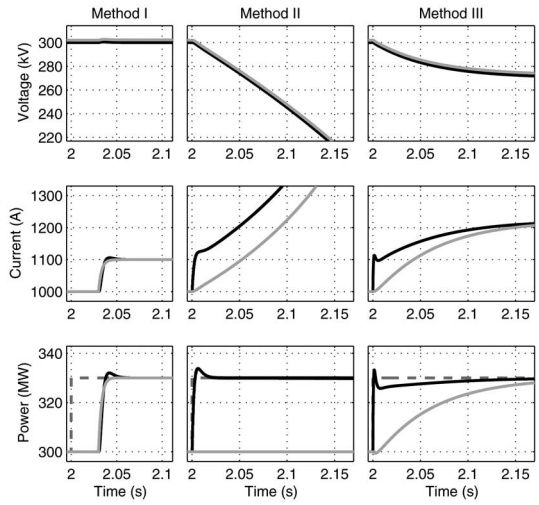

Fig. 5. Response to a change in power order for Methods I–III; showing dc-link voltage, current, and power. The black line corresponds to the GS-VSC and gray line corresponds to the WF-VSC. The dashed line shows the power order.

TABLE I
Simulation Model Parameters

Parameter	Value	Units
Nominal HVDC voltage	300	kV
Nominal HVDC current	1000	A
WF rated power	300	MW
HVDC link capacity	200	μF
HVDC cable resistance	2	Ω
Frequency response power margin	0.1	p.u.
HVDC voltage margin	0.1	p.u.
Total communication delay	30	ms
Wind turbine current control settling time	10	ms
VSC-HVDC current control settling time	3	ms
Method III reference settling time	180	ms

B. Method II: Response From the Energy of the HVDC Link

The frequency of the grid is obtained by the GS-VSC, a power order is calculated, and the required power is injected to the grid by taking stored energy in the capacitance of the HVDC link, which is achieved by changing its voltage. The energy stored in the HVDC link $E_{\rm dc}$ and the power extracted from it $P(t)$ can be written as

$$E_{\rm dc}(t) = \frac{1}{2}CV_{\rm dc}(t)^2, \quad P(t) = CV_{\rm dc}(t)\frac{d}{dt}V_{\rm dc}(t). \tag{8}$$

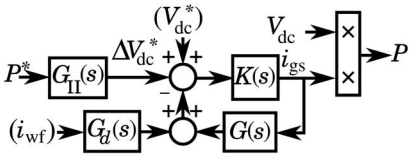

Fig. 6. Block diagram of Method II.

The variation of the voltage required to track a power reference can be obtained as

$$V_{\rm dc}^*(t) = \sqrt{\left(V_{\rm dc}^N\right)^2 - \frac{2}{C}\int P^*(t)dt} \approx V_{\rm dc}^N - \frac{1}{CV_{\rm dc}^N}\int P^*(t)dt. \quad (9)$$

By linearizing the equation for small variations of the $V_{\rm dc}$, the following transfer function is obtained:

$$\Delta V_{\rm dc}^*(s) = \underbrace{-\frac{1}{CV_{\rm dc}^N}\frac{1}{s}}_{G_{\rm II}(s)} P^*(s). \quad (10)$$

The complete diagram is shown in Fig. 6. The resulting relation between the power order and its actual value is

$$P(s) \approx V_{\rm dc}^N K(s) G_S(s) G_{\rm II}(s) P^*(s). \quad (11)$$

From (10), it becomes apparent that a sustained power injection would cause a sustained voltage drift. Such situation is illustrated in Fig. 5, where Method II has been applied to the same system described earlier. This is not an issue if the system is used to provide only the inertial response, as proposed in [13], as the energy stored in the HVDC link would play the role of the kinetic energy in a conventional power plant. By combining the inertia emulation equation (4) with the power extracted from the capacity (8) the following relation is found:

$$V_{\rm dc}(t) = \sqrt{\left(V_{\rm dc}^N\right)^2 + \frac{2HS^N}{C}\frac{f^2 - \left(f^N\right)^2}{\left(f^N\right)^2}} \approx \sqrt{\left(V_{\rm dc}^N\right)^2 + \frac{4HS^N}{C}\frac{f - f^N}{f^N}}. \quad (12)$$

Thus, in a system with a properly chosen capacity and emulated inertia time, the voltage of the HVDC link would be kept in a safe operating range as long as a major frequency collapse did not occur in the ac grid. The following expressions show the tradeoffs between the capacity of the HVDC link, the maximum allowed HVDC voltage deviation $\Delta V_{\rm dc}$, and the emulated inertial time for a given maximum expected frequency error Δf:

$$C = \frac{2HS^N}{V_{\rm dc}^N \Delta V_{\rm dc}}\frac{\Delta f}{f^N} \quad (13)$$

$$\Delta V_{\rm dc} = \frac{2HS^N}{C}\frac{1}{V_{\rm dc}^N}\frac{\Delta f}{f^N} \quad (14)$$

$$H = \frac{C}{2}\frac{f^N}{\Delta f}\frac{V_{\rm dc}^N \Delta V_{\rm dc}}{S^N}. \quad (15)$$

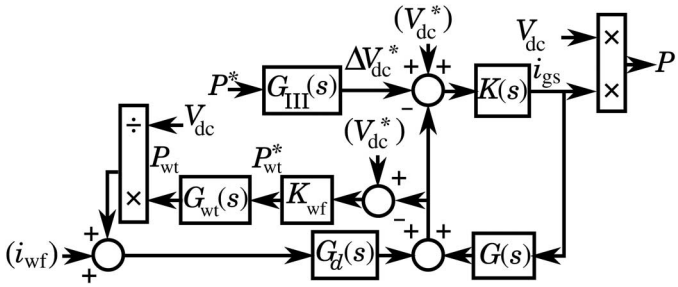

Fig. 7. Block diagram of Method III.

The main benefit of this method is that the system is capable of providing a very quick inertial response toward the ac grid without requiring support from the wind turbines, as shown in Fig. 5. However, the energy stored in the HVDC link required to produce an inertia time comparable to a conventional power plant is very high compared to the capacity that is normally available in VSC-HVDC systems. For example, for the system described in Table I, the emulated inertia, considering a maximum frequency deviation of 1 Hz and a maximum voltage deviation of 10%, would be $H = 0.15$ s, which is very low [1]. In order to achieve an inertia of $H = 2.5$ s, which is a low boundary of the usual range for thermal plants, the minimum capacity required would be $C = 3.33$ mF. This would require multiplying by a factor of 17 the HVDC link capacitance.

C. Method III: HVDC Energy Buffer With WF Support

Method III is new method that uses a combination of the energy stored in the capacitance of the HVDC link plus the power injected by the WF-VSC to provide frequency support. When a frequency deviation requiring the support is detected, the setpoint for the voltage of the link is reduced, such that the energy is released from link capacitance in a similar manner like Method II. However, unlike Method II, on detecting the reduced voltage, the WF-VSC adjusts the power order of the WF to access WF kinetic energy. The initial voltage reduction delivers the first package of response energy which is gradually supplemented by the kinetic energy of the wind turbines in a way that does not require a fast response from the turbines, unlike Method I, nor high energy storage capacity in the link, unlike Method II. The method has the added benefit of not requiring communication between the GS-VSC and the WF-VSC, as the WF-VSC detects the requirement to change the power order of the WF based on the voltage measured in the link.

The block diagram of the control scheme is shown in Fig. 7. The variation of the voltage order of the GS-VSC $\Delta V_{\rm dc}^*$ is obtained from the required power reference as

$$\Delta V_{\rm dc}^* = \underbrace{-\frac{1}{CV_{\rm dc}^N}\frac{\tau}{\tau s + 1}}_{G_{\rm III}(s)} P^*(s) \quad (16)$$

where τ is a design parameter, a time constant, that affects the resulting variation of the dc voltage and the performance requirements of the WF.

The power order of the WF-VSC is modified using a proportional controller $K_{\rm wf}$ fed with the voltage error of the link

$$P^*_{\rm wt} = \underbrace{\frac{CV^N_{\rm dc}}{\tau}}_{K_{\rm wf}} \left(V^N_{\rm dc} - V_{\rm dc}\right). \tag{17}$$

The resulting transfer function between the power reference and the actual power injected to the grid is

$$\begin{aligned} P(s) \approx\ & V^N_{\rm dc} KS(s) G_{\rm III}(s) P^*(s) \\ & + V^N_{\rm dc} KS(s) G_d(s) \frac{1}{V^N_{\rm dc}} G_{\rm wt}(s) K_{\rm wf} G_T(s) \\ & \times G_{\rm III}(s) P^*(s) \end{aligned} \tag{18}$$

where the first term corresponds to the power extracted from the energy stored in the link, and the second term corresponds to the support provided by the WF.

If the bandwidth of $G_{\rm III}(s)$ is chosen to be low enough, by making τ greater than the time constants of the HVDC link voltage regulator and the wind turbine tracking dynamics, the previous transfer functions can be simplified because $G_{wt}(s)G_T(s)G_{\rm III}(s) \approx G_{\rm III}(s)$. Further, as the voltage regulator is designed to reject disturbances at low frequencies, $KS(s) \approx G(s)^{-1}$ [15]. Then, the previous equation becomes

$$\begin{aligned} P(s) \approx\ & V^N_{\rm dc} G(s)^{-1} G_{\rm III}(s) P^*(s) \\ & + V^N_{\rm dc} G(s)^{-1} G_d(s) \frac{1}{V^N_{\rm dc}} K_{\rm wf} G_{\rm III}(s) P^*(s) \end{aligned} \tag{19}$$

which is equivalent to

$$P(s) \approx \underbrace{\frac{\tau s}{\tau s + 1} P^*(s)}_{\text{from HVDC energy}} + \underbrace{\frac{1}{\tau s + 1} P^*(s)}_{\text{from WF}} = P^*(s). \tag{20}$$

The resulting response, simulated using the same system as in Sections II-A and II-B, is shown in Fig. 5. Notice that the system is capable of providing a fast response comparable to Method II with a comparatively smaller variation of the voltage. Further, the wind turbines are not required to ramp up their power output as quick as in Method I while delivering the required power to the grid earlier.

Choosing the large value of τ has been shown to reduce the required wind turbine reference tracking performance; however, it also produces a greater deviation of the voltage of the link. The relation between the maximum allowable voltage deviation $\Delta V_{\rm dc}$, the power headroom available ΔP, and the time constant τ can be obtained from (16)

$$\Delta V_{\rm dc} = \frac{\tau}{CV^N_{\rm dc}} \Delta P. \tag{21}$$

It is also useful to put the previous relation as a function of the inertia time and the ROCOF $\dot{f}_R$ from (4)

$$\Delta V_{\rm dc} = \frac{\tau}{CV^N_{\rm dc}} \frac{2HS^N}{f^N} \dot{f}_R \tag{22}$$

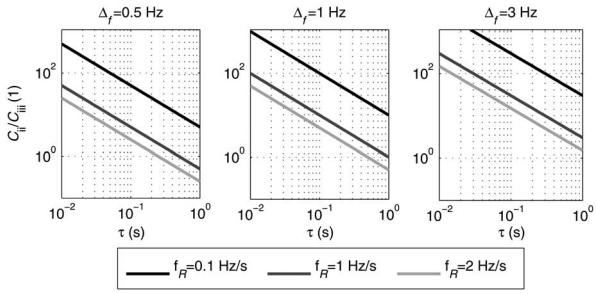

Fig. 8. Capacitance required by Method II against the capacitance required by Method III for different values of Δ_f, $\dot{f}_R$, and τ.

also

$$C = \frac{2HS^N}{V^N_{\rm dc} \Delta V_{\rm dc}} \frac{\tau \dot{f}_R}{f^N} \tag{23}$$

$$\tau = \frac{C}{2} \frac{V^N_{\rm dc} \Delta V_{\rm dc}}{2HS^N} \frac{f^N}{\dot{f}_R}. \tag{24}$$

Following the example used in Method II, considering the requirement to provide an emulated inertia of $H = 2.5$ s, with a 10% margin for voltage deviation and a maximum ROCOF of 1 Hz/s, the original VSC-HVDC system with $C = 200$ μF would be capable of providing the desired inertia, giving the wind turbines a settling time of 0.18 s to react, i.e., $3\tau = 0.18$ s.

Equation (23) can be used to compare the sizing requirements of the new method with the requirements of Method II from (13). The ratio between the capacitance required by Method II $C_{\rm II}$ and the capacitance required by Method III $C_{\rm III}$ is

$$\frac{C_{\rm II}}{C_{\rm III}} = \frac{\Delta_f}{\tau \dot{f}_R}. \tag{25}$$

Note that this ratio only depends on the maximum expected frequency error Δ_f, the maximum expected ROCOF $\dot{f}_R$, and the time given to the WF to react in Method III, 3τ; also, it neither depends on the emulated inertia time nor the allowed voltage margin. A plot of this ratio is shown in Fig. 8. The values of Δ_f have been chosen following the System Operator Transmission Owner Code from U.K. National Grid, which requires operating HVDC links at frequencies as low as 47 Hz [16]. The values of the ROCOF have been set following the $1\ \text{Hz} \cdot \text{s}^{-1}$ ROCOF protection setting recently proposed for generators over 5 MW in a recent Industry Consultation by U.K. National Grid [17].

The plot suggests that Method III is a better alternative than Method II unless long WF response times are desired. For low values of τ, Method III requires several orders of magnitude less capacitance than Method II. However, note that if very fast reaction times of the WF are required, the benefits of Method III compared to Method I would be lost and the assumptions in the derivation of (19) would not be correct.

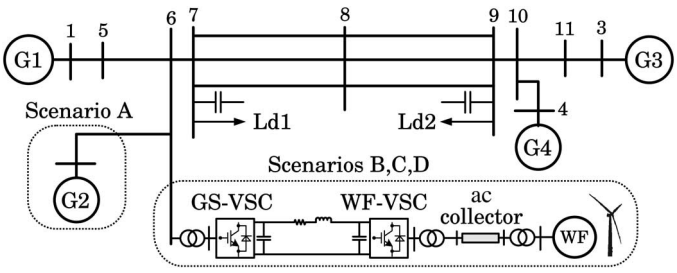

Fig. 9. 4-Machine, 2-area test network. G1–G4 represent conventional generators in Scenario A. G2 is replaced by an equivalent offshore WF for Scenarios B, C, and D.

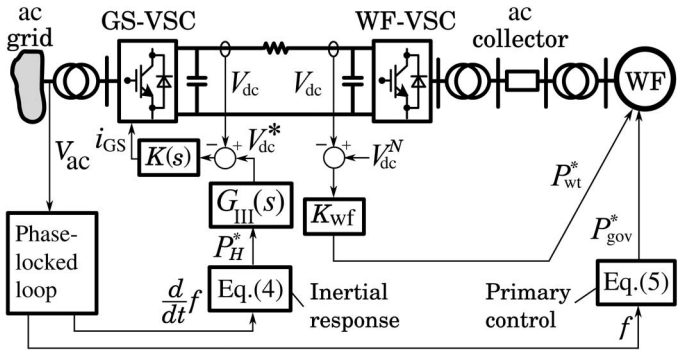

Fig. 10. Representation of the HVDC-connected offshore WF with the proposed control strategy (Method III) for inertial response (simulated in Scenarios C and D) along with primary control (Scenarios B and C).

V. Evaluation of the Proposed Method Using a Dynamic Power System Model

In order to further substantiate the benefits of the proposed method, a series of case studies are presented in the next section considering detailed dynamic simulation models for the ac system, wind turbines, and HVDC link, developed in DIgSILENT PowerFactory.

A. System Description

The ac system model is based on the well-known test system with four machines and two areas described in [1]. Several modifications have been made to the original system to suit the presented case study. Three tie lines as shown in Fig. 9 are considered. Each area consists of two coupled generation units, each having a rating of 600 MVA and 20 kV output voltage. Frequency-dependent load models are considered. In steady state, each unit dispatches 500 MW with the loads $Ld1 = 600$ MW and $Ld2 = 1358$ MW resulting in a tie line flow of 380 MW (bus 7–9).

Four different scenarios are studied.

- *Scenario A:* Conventional generation, no WF.
- *Scenario B:* Displacement of a conventional power plant by an offshore WF (no inertial support, with primary control).
- *Scenario C:* Displacement of a conventional power plant by an offshore WF (with inertial support, with primary control).
- *Scenario D:* Displacement of a conventional power plant by an offshore WF (with inertial support, without primary control).

1) Scenario A: In this scenario, all the generators are synchronous machines from conventional thermal plants equipped with steam turbine-governor systems [1].

2) Scenario B: The base case described above is modified by replacing a conventional power plant (G2) with an offshore WF radially connected to bus 6 via a ± 150 kV symmetric monopole VSC-HVDC link with length 100 km. The WF comprises 367 wind turbines rated at 1.5 MVA and 0.69 kV output voltage, aggregated and represented by WF, as shown in Fig. 9. An over-provision of up to 10% of the rated turbine power is specified. Thus, considering the available overload capability (headroom), the wind turbines can operate at a maximum of 550 MW. At full load (under normal operation), the WF transfers 500 MW through a 33-kV ac feeder on to the GS-VSC. The doubly fed induction generators are simulated using an aggregated model based on the dynamic model of the General Electric (GE) 1.5 MW WTG described in [18]. The model contains a two-mass lumped parameter model of the mechanical system and an averaged model of the power converter with their corresponding controllers.

Both GS-VSC and WF-VSC are rated at 550 MVA. The WF-VSC converter operates in ac voltage control as a slack bus to allow for the wind active power to transfer onto the HVDC link. The GS-VSC operates in $V_{\rm dc} - V_{\rm ac}$ mode, maintaining constant dc bus voltage and ac voltage control at the PCC, as shown in Fig. 10. Decoupled current control strategy in the modified reference frame ($d'q'$) and standard PI controllers were used in the converter, which was simulated using an averaged model [19], [20].

In general, wind generators do not contribute to primary frequency control, as it is more economical to maintain reserve on more conventional units (hydro and thermal). An example where such functionality has been demonstrated is the Horns Rev offshore WF in Denmark [21], which demonstrates various control features including a reserve capability (i.e., it is possible to operate the WF to maintain, e.g., 5% reserve margin that may be called upon during a frequency decline). In a transmission system where wind is likely to be a major portion of the generation mix (typically small and islanded systems), both inertial response and primary frequency control may become necessary.

Scenario B considers the case whereby the HVDC-connected offshore WFs contribute toward primary frequency response, as shown in Fig. 10. The primary frequency control uses a similar scheme which was adopted for the conventional generators. Further details can be obtained in [1]. The frequency is measured at the GS-VSC and communicated to the WF site.

3) Scenario C: The proposed inertia emulation control scheme (Method III) is implemented as described in Section IV-C. The parameters of the inertia emulation are chosen considering a maximum acceptable deviation of the HVDC link voltage of 10%, a WF reference tracking settling time of 180 ms ($\tau = 60$ ms), an emulated inertia time of $H = 8.5$ s (considering $S^N = 500$ MVA) chosen to match that of the replaced generator, and a maximum expected ROCOF $\dot{f}_R = 0.35$ Hz/s.

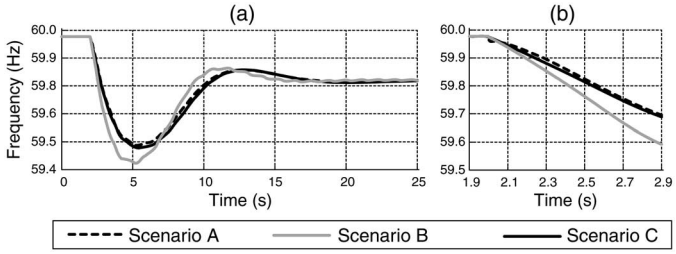

Fig. 11. Transient response of the frequency to a sudden change of the load under Scenarios A, B, and C. The complete transient is shown in (a) and the initial transient, where inertial response plays an important role, is magnified in (b).

4) Scenario D: This scenario is the same as Scenario C with the exception that the primary control support is not in operation.

VI. Results and Discussion

Time-domain simulations for a sudden increase in the loading of the power system (25% increase of Ld1) were carried out to compare the system recovery performance under different scenarios.

The frequency of the grid, shown in Fig. 11, follows a classical power system transient in all scenarios. This transient is characterized by an initial drop of the frequency at a constant rate followed by a recovery (starting near $t = 5$ s) and a stabilization of the frequency with a certain steady-state error. The results show that without inertia emulation (Scenario B), the ROCOF during the initial drop becomes 33% faster compared to Scenario A due to 25% reduction of the overall system inertia. In contrast, inertia emulation in Scenario C allows to preserve the same initial ROCOF as in Scenario A. This is apparent by observing the zoomed-in Fig. 11(b).

The active power involved in the transient response of the system is shown in Fig. 12. Comparing G2 from Scenario A with the GS-VSC from Scenario C in Fig. 12(a) and (b), it can be seen that their power injection follows a similar transient with small differences due to a superimposed oscillation representing lightly damped modes of the system. When the sudden step in the load occurs at time 2 s, both generators change in stepwise their active power due to their inertial response following the derivative of the frequency without significant effect of the primary control. This is further confirmed by comparing the initial response of Scenarios C and D (where the primary control is not in operation) in Fig. 13. By comparing the power injected by the GS-VSC with the power coming from the WF onto the dc link in Fig. 12(b) and (d), during the initial transient, the ability of Method III to provide a sudden response toward the ac grid while giving the WF time to react is also validated.

The effect of having primary control is shown in Fig. 13, where Scenarios C and D are compared. The transient response of the frequency in Fig. 13(a) shows that the inertia emulation alone is responsible for providing support during the first few seconds of the transient, whereas the primary response effect can be seen afterwards as discussed earlier.

The variation of the dc-link voltage is shown in Fig. 12(e) and (f). It can be seen that the voltage follows a transient

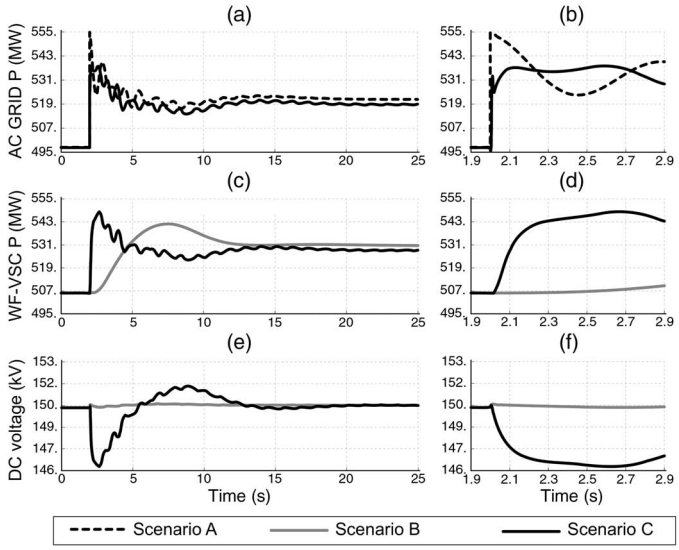

Fig. 12. Transient response of the active power to a sudden change of the load. Scenario A versus scenario C is shown in (a). A comparison of the power going from the WF onto the dc link (Scenarios B and C) is shown in (b). The variation of the dc-link voltage is shown in (c) showing the effect of using Method III in Scenario C. A magnification of the transients during the first second is shown to the right.

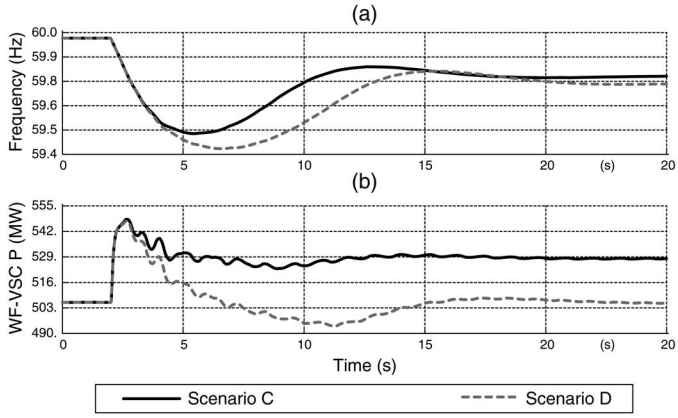

Fig. 13. Response to a change in power order for Methods I–III; showing dc-link voltage, current, and power. The black line corresponds to the GS-VSC and gray line corresponds to the WF-VSC. The dashed line shows the power order.

which resembles the derivative of the frequency of the grid in Scenario C as expected, without exceeding the specified operational limits. It is also worth noticing that voltage error in the dc link only occurs during the fast transient response of the frequency, reaching zero once the frequency stabilizes. This is a further advantage of the proposed method (Method III) as opposed to Method II. The justification for this is, having a voltage reduction in steady state, while the grid frequency requires action from the secondary control to recover its nominal value, would require higher current in the dc link, thus higher losses and potentially higher costs.

VII. Conclusion

This paper presents a new method that allows remote offshore WFs connected through VSC-HVDC links to participate in ac grid frequency control by blending the energy storage

capability of the HVDC link and the frequency support capabilities of wind turbines. The blended approach has numerous advantages compared to the already existing methods as it allows to obtain an almost instantaneous response toward the ac grid, keeping the performance requirements of the wind turbines low without requiring a significant increase of the volume of the capacitors of the HVDC power converters.

REFERENCES

[1] P. Kundur, *Power System Stability and Control*. New York, NY, USA: McGraw-Hill, 1994.

[2] P. W. Christensen *et al.*, "Generic grid code format for wind power plants," European Wind Energy Association, Belgium, Tech. Rep., 2009.

[3] R. J. Piwko *et al.*, "Interconnection requirements for variable generation," North American Electric Reliability Corporation (NERC), Atlanta, GA, USA, Tech. Rep., 2012.

[4] J. M. MacDowell, K. Clark, N. W. Miller, and J. J. Sanchez-Gasca, "Validation of GE wind plant models for system planning simulations," in *Proc. IEEE Power Energy Soc. Gen. Meeting*, 2011, pp. 1–8.

[5] G. C. Tarnowski, "Systems and methods for generating an inertial response to a change in the voltage of an electrical grid," U.S. Patent US 2012/0 310 426 A1, December 06, 2012.

[6] J. Ekanayake and N. Jenkins, "Comparison of the response of doubly fed and fixed-speed induction generator wind turbines to changes in network frequency," *IEEE Trans. Energy Convers.*, vol. 19, no. 4, pp. 800–802, Dec. 2004.

[7] J. Morren, J. Pierik, and S. W. De Haan, "Inertial response of variable speed wind turbines," *Electr. Power Syst. Res.*, vol. 76, no. 11, pp. 980–987, 2006.

[8] J. F. Conroy and R. Watson, "Frequency response capability of full converter wind turbine generators in comparison to conventional generation," *IEEE Trans. Power Syst.*, vol. 23, no. 2, pp. 649–656, May 2008.

[9] G. C. Tarnowski, P. C. Kjær, P. E. Sørensen, and J. Østergaard, "Study on variable speed wind turbines capability for frequency response," in *Proc. Eur. Wind Energy Conf.*, 2009, pp. 16–19.

[10] Y. Pipelzadeh, B. Chaudhuri, and T. C. Green, "Inertial response from remote offshore wind farms connected through VSC-HVDC links: A communication-less scheme," in *Proc. IEEE Power Energy Soc. Gen. Meeting*, 2012, pp. 1–6.

[11] Y. Phulpin, "Communication-free inertia and frequency control for wind generators connected by an HVDC-link," *IEEE Trans. Power Syst.*, vol. 27, no. 2, pp. 1136–1137, May 2012.

[12] B. Silva, C. Moreira, L. Seca, Y. Phulpin, and J. Peas Lopes, "Provision of inertial and primary frequency control services using offshore multiterminal HVDC networks," *IEEE Trans. Sustain. Energy*, vol. 3, no. 4, pp. 800–808, Oct. 2012.

[13] J. Zhu, C. D. Booth, G. P. Adam, A. J. Roscoe, and C. G. Bright, "Inertia emulation control strategy for VSC-HVDC transmission systems," *IEEE Trans. Power Syst.*, vol. 28, no. 2, pp. 1277–1287, May 2013.

[14] J. Machowski, J. Bialek, and J. Bumby, *Power System Dynamics: Stability and Control*. Hoboken, NJ, USA: Wiley, 2008.

[15] S. Skogestad and I. Postlethwaite, *Multivariable Feedback Control*. Hoboken, NJ, USA: Wiley, 2005.

[16] (2014, Aug. 1) *The System Operator-Transmission System Owner Code (STC)* [Online]. Available: www2.nationalgrid.com/UK/Industry-information/Electricity-codes/System-Operator-Transmission-Owner-Code

[17] D. Spillett, "Frequency changes during large disturbances and their impact on the total system," National Grid, Tech. Rep. GC0035, Aug. 2013 .

[18] N. Miller, J. J. Sanchez-Gasca, W. Price, and R. Delmerico, "Dynamic modeling of GE 1.5 and 3.6 MW wind turbine-generators for stability simulations," in *Proc. IEEE Power Eng. Soc. Gen. Meeting*, 2003, vol. 3, pp. 1977–1983.

[19] C. Schauder and H. Mehta, "Vector analysis and control of advanced static VAR compensators," *Proc. IEEE Gen. Transm. Distrib.*, vol. 140, no. 4, pp. 299–306, 1993.

[20] Y. Pipelzadeh, B. Chaudhuri, and T. Green, "Control coordination within a VSC HVDC link for power oscillation damping: A robust decentralized approach using homotopy," *IEEE Trans. Control Syst. Technol.*, vol. 21, no. 4, pp. 1270–1279, Jul. 2013.

[21] P. Pourbeik, "Modeling and dynamic behavior of wind generation as it relates to power system control and dynamic performance," CIGRE, Paris, France, Tech. Brochure 328, WG C4.601, Aug. 2007.

Adrià Junyent-Ferré (S'09–M'11) received the B.Sc. and M.Sc. degrees in industrial engineering from the School of Industrial Engineering of Barcelona (ETSEIB), Technical University of Catalonia (UPC), Barcelona, Spain, in 2007, and the Ph.D. degree in electrical engineering from the UPC, in 2011.

He was a Researcher with Centre d'Innovació Tecnològica en Convertidors Estàtics i Accionaments (CITCEA-UPC) from 2006 to 2012 and a Lecturer with Barcelona College of Industrial Engineering (EUETIB) in 2012. He joined the Department of Electrical and Electronic Engineering, Imperial College London, London, U.K., as a Research Associate, in 2013 and was appointed as a Lecturer in HVDC Power Transmission in 2014. His research interests include control of power electronic converters for large scale renewable power generation and HVDC power transmission.

Yousef Pipelzadeh (S'09–M'13) received the M.Eng. degree (first class hons.) in communications systems engineering from Swansea University, Swansea, U.K., in 2007, and the Ph.D. degree in system aspects of wind and HVDC from Imperial College London, London, U.K., in 2012.

He worked with Wesley Clover International Corporation, Kanata, Canada, from 2007 to 2008. He is currently a Research Associate with Imperial College London. His research interests include power system dynamics and stability, HVDC transmission, and offshore dc networks.

Dr. Pipelzadeh is an active member of Conseil International des Grands Réseaux Électriques (CIGRÉ) and the Institution of Engineering and Technology (IET).

Tim C. Green (M'89–SM'02) received the B.Sc. (Eng.) (first class hons.) degree from Imperial College London, London, U.K., in 1986, and the Ph.D. degree from Heriot-Watt University, Edinburgh, U.K., in 1990, both in electrical engineering.

He is a Chartered Engineer in the U.K. He was a Lecturer with Heriot-Watt University, Edinburgh, U.K., until 1994, and is now a Professor of Electrical Power Engineering with Imperial College London, Deputy Head of the Electrical and Electronic Engineering Department, and Director of the Energy Futures Laboratories, Imperial College London. He leads the HubNet consortium of eight U.K. universities coordinating research in low-carbon energy networks and is the Network Champion for the Research Councils U.K. His research interests include formulating the future form of the electricity network to support low-carbon futures, in offshore dc networks, and management of low-voltage networks. A particular theme is how the flexibility of power electronics and control can be used to accommodate new generation patterns and new forms of load, such as EV charging, as part of the emerging smart grid.